Distributed energy storage control for dynamic load impact mitigation

Submitted to *Energies*. Pages 1 - 20.

OPEN ACCESS

Article

Distributed Energy Storage Control for Dynamic Load Impact Mitigation

Maximilian J. Zangs [1,†], Peter B. E. Adams [1,†], Dr Timur Yunusov [1], Dr William Holderbaum [1*] and Dr Ben A. Potter [1]

[1] School of Systems Engineering, University of Reading, Whiteknights Campus, RG6 6AY, Reading, United Kingdom

† These authors contributed equally to this work.

* Author to whom correspondence should be addressed; w.holderbaum@reading.ac.uk, Tel: +44 1183 786086, Fax: +44 1189 751994

Version January 30, 2016 submitted to Energies. *Typeset by LaTeX using class file mdpi.cls*

Abstract: The future uptake of Electric Vehicles (EV) in low-voltage distribution networks can cause increased voltage violations and thermal overloading of network assets, especially in networks with limited headroom at times of minimum or peak demand. To address the problem, this paper proposes a distributed battery energy storage solution, controlled using an Additive Increase Multiplicative Decrease (AIMD) algorithm. The proposed AIMD+ algorithm uses local voltage measurements and a reference voltage threshold to determine the Additive Increase parameter and to control the charging and discharging of the battery. The voltage threshold used is dependent on the network topology and is calculated using power flow analysis, with peak demand equally allocated between loads. Simulations were performed on the IEEE European test case and a number of real UK suburban networks, using European demand data and a realistic electric vehicle travel model. The performance of the standard AIMD algorithm with fixed voltage threshold and the proposed AIMD+ algorithm with reference voltage profile are compared. Results show that, compared to the standard AIMD case, the proposed AIMD+ algorithm improves the voltage profile, reduces thermal overloads and ensures fairer battery utilisation.

Keywords: Battery storage; Distributed control; Electric vehicles; AIMD; Voltage control; Smart grid

---

1. Introduction

The adoption of Electric Vehicles (EV) is seen as a potential solution to the decarbonisation of future transport network, offsetting emissions from conventional internal combustion engine vehicles. Current rate of EV uptake is anticipated to increase with improved driving range, reduced cost of purchase and greater emphasis on leading an environmentally friend lifestyle [1]. It is predicted that by 2030, there will be three million Plug-in Hybrid Electric Vehicles and EVs sold in Great Britain and Northern Ireland [2], and it is expected that by 2020 every tenth car in the United Kingdom will be electrically powered [3]. It is anticipated that the majority of PHEV/EV will be charged at home, which puts additional stress on the existing local low voltage distribution network, which must provide the increased demand in energy [4,5]. Uncontrolled charging of multiple PHEV/EV raises the daily peak power demand, which leads to: increased transmission line losses, higher voltage drops, equipment overload, damage, and failure [6–9]. Accommodating the increased demand and mitigation of such failures is a major area of research interest, with the focus mainly placed on the coordinating and support of home-charging.

Demand Side Management (DSM) strategies, that aim to alleviate the impacts of PHEV/EV home-charging, are a favoured solution. Mohsenian-Rad *et.al.* in [10] developed a distributed DSM algorithm that implicitly controls the operation of loads, based on game theory and the network operator's ability to dynamically adjust energy prices. Focusing on financial incentive driven DSM strategies, in [11], a time-of-use (TOU) tariff and real-time load management strategy was proposed, where disruptive charging is avoided by allocating higher prices to times of peak demand. In addition, Distributed Generation (DG) has also been included with the optimisation of PHEV/EV charging using financial incentives [12].

Research focused on grid support has been driven by the need to deliver long term savings and to avoid the immediate costs and disruption of network reinforcements and upgrades. This research proposes the implementation of alternative solutions to support the adoption of low carbon technologies, such as Electric Vehicles and Heat pumps. To reduce the occurrence increased peak demands, Mohsenian-Rad *et.al.* developed an approach of direct interaction between grid and consumer to achieve valley-filling, by means of dynamic game theory [10]. In [13], a MAS was used to manage flexible loads for the minimisation of cost in a dynamic game. The use of aggregators has been proposed to allow the participation of a number of small providers to participate in network support, such as grid frequency response [14–16].

Research focused on grid support has been driven by the need to deliver long term savings and to avoid the immediate costs and disruption of network reinforcements and upgrades. This research proposes the implementation of alternative solutions to support the adoption of low carbon technologies, such as Electric Vehicles and Heat pumps. To reduce the occurrence increased peak demands, Mohsenian-Rad *et.al.* developed an approach of direct interaction between grid and consumer to achieve valley-filling, by means of dynamic game theory [10]. In [13], a MAS was used to manage flexible loads for the minimisation of cost in a dynamic game. The use of aggregators has been proposed to allow the participation of a number of small providers to participate in network support, such as grid frequency response [14–16].

In this paper, a similar approach to support electricity distribution feeders is proposed, where dedicated energy storage units mitigate the effects of disruptive loads, such as the high uptake of Electric Vehicles. An Additive Increase Multiplicative Decrease (AIMD) type algorithm is proposed for control of the battery energy storage devices. AIMD algorithms were originally applied to congestion management in communications networks using the TCP protocol[17], to maximise utilisation while ensuring a fair allocation of data throughput amongst a number of competing users. AIMD-type algorithms have been applied to power sharing scenarios in low voltage distribution networks, where the limited resource is the availability of power from the substation's transformer. An AIMD-type algorithm was first proposed for EV Charging by Stüdli *et.al.* [18], requiring a one-way communications infrastructure to broadcast a 'capacity event', this was further developed to include vehicle-to-grid applications with reactive power support [19,20]. The proposed battery control algorithm builds upon work by Mareels *et.al.* [21], to include bidirectional power flow and the use of a reference voltage profile derived from network models.

The remainder of this paper is organised as follows: Section 2 outlines the EV, network and storage models used in the research. Additionally it explains the assumptions that accommodate and validate these models. Section 3 elaborates on the proposed AIMD control algorithm (AIMD+). Next, Section 4 details the implementation and scenarios used for particular test cases that. For later comparison, this section also outlines a set of comparison metrics. Section 5 presents and discusses the results, followed by the conclusion in Section 6.

2. System Modelling

In this section, the underlying assumptions to validate the research are addressed. Next, a model to describe Electric Vehicle charging behaviour is explained. This is followed by a model of the battery energy storage. Finally, the network models used to simulate the power distribution networks are explained.

2.1. Assumptions

For this work several underlying assumption were made to generate the models:

1. The uptake of EVs is assumed to increase and hence have a significant impact on the normal operation of the low voltage distribution network. This assumption is based on a well established prediction that the majority of EV charging will take place at home [22].
2. The transition from internal combustion engine powered vehicles to EVs is assumed to not impact the users' driving behaviour. Similar to [23], this assumption allows the utilisation of recent vehicle mobility data [24] to generate leaving, driving and arriving probabilities, from which the EV charging demand can be determined.
3. The transition to low carbon technologies will likely increase the variability and flexibility of demand and so support devices, such as battery energy storage, are anticipated to play a more important role. Hence, alongside a high uptake of Electric Vehicles, an increased adoption of distributed energy storage devices is assumed.

4. It is assumed that energy storage solutions, or more specifically battery storage solutions, start the simulations at 50% SOC and are not 100% efficient at storing and releasing electrical energy, as in [25]. Additionally, its utilisation will degrade the energy storage capability and performance over time as shown in [26]. Therefore the requirements for fair storage usage is of primary importance.

5. It is assumed that the load profiles provided by the IEEE Power and Energy Society (PES) are sufficient as base load profiles for all simulations.

2.2. Electric Vehicle Charging Behaviour

From publicly available car mobility data [23,24] an empirical model was developed to capture the underlying driving behaviour. The raw data, $n_r(t)$, represents the probabilities of starting a trip during a 15 minutes period of a weekday. Three continuous normal distribution functions, each defined as:

$$\hat{n}_x(t) = \beta_x \frac{1}{\sigma_x\sqrt{2\pi}} \exp\left[-\frac{\left({}^{t}\!/_{24} - \mu_x\right)^2}{2\sigma_x^2}\right] \quad \text{where } t = [0, 24] \tag{1}$$

were used to represent vehicles leaving in the morning, $\hat{n}_m(t)$, lunch time, $\hat{n}_l(t)$, and in the evening, $\hat{n}_e(t)$. The aggregate probability of these three functions was optimised using a Generalised Reduced Gradient (GRG) algorithm to fit the original data. In order to represent a symmetric commuting behaviour, i.e. vehicles departing in the morning return during the evening, an equality amongst the three probabilities was defined as follows:

$$0 = \int_0^{24} \left[\hat{n}_m(t) + \hat{n}_l(t) - \hat{n}_e(t)\right] dt \tag{2}$$

The resulting parameters from the GRG fitting of the three distribution functions are tabulated in Table 1. Additionally, the resulting departure probabilities, as well as the reference data $n_r(t)$ are shown in Figure 1.

Table 1. Parameters for normal distributions

Equation $\hat{n}_x(t)$	μ_x (mean)	σ_x (Std. Dev.)	β_x (weight)
$\hat{n}_m(t)$	0.3049	0.0488	0.00206
$\hat{n}_l(t)$	0.4666	0.0829	0.00314
$\hat{n}_e(t)$	0.7042	0.0970	0.00521

Statistical data capturing the probability distribution of a trip being of a certain distance was also extracted from the dataset. This was done for both the weekdays $w_{wd}(d)$ and weekends $w_{we}(d)$. The Weibull function was chosen to be fitted against the extracted probability distributions, and is defined as:

$$\hat{w}_x(d) := \begin{cases} \frac{k_x}{\gamma_x}\left(\frac{d}{\gamma_x}\right)^{k_x-1} \exp\left[-\left(\frac{d}{\gamma_x}\right)^{k_x}\right] & \text{if } d \geq 0 \\ 0 & \text{if } d < 0 \end{cases} \tag{3}$$

Performing the curve fitting using the GRG optimisation algorithm, a weekday trip distances distribution, $\hat{w}_{wd}(d)$, and a weekend trip distribution, $\hat{w}_{we}(d)$ could be estimated. The computed

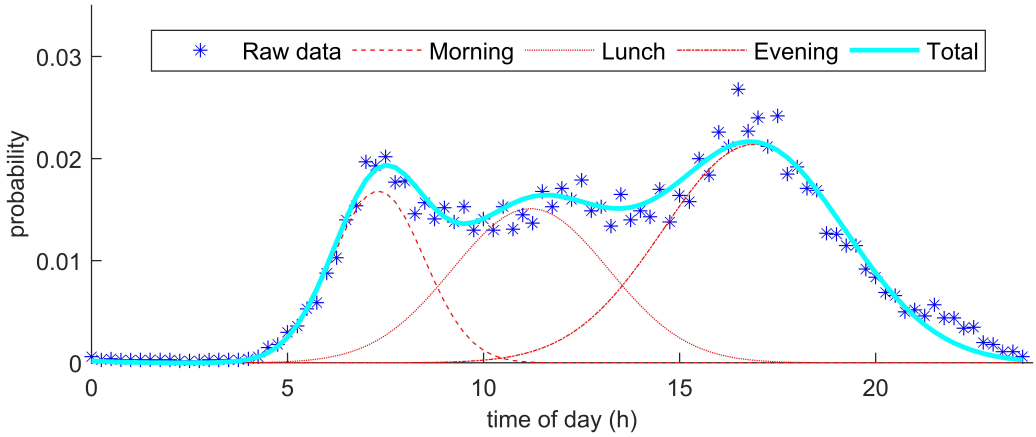

Figure 1. The probability of starting a trip at a particular time during a weekday, extrapolated into three normal distributions (RMS error: 9.482%).

function parameters for these two estimated distribution functions are tabulated in Table 2. Their resulting probability distributions are plotted for comparison against the real data in Figure 2.

Table 2. Parameters for Weibull distributions

Equation $\hat{w}_x(d)$	γ_x (scale)	k_x (shape)
$\hat{w}_{wd}(t)$	15.462	0.6182
$\hat{w}_{we}(t)$	38.406	0.4653

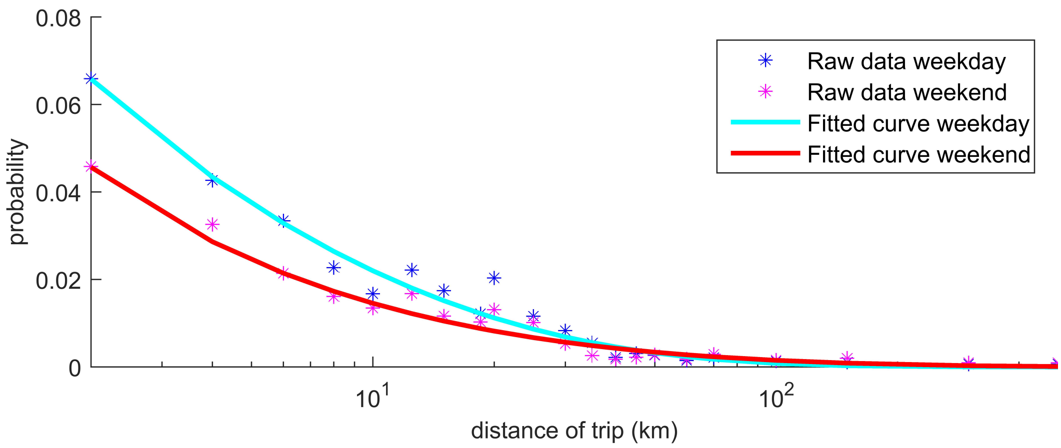

Figure 2. The probability of a trip being of a particular distance during a weekday, extrapolated into a Weibull distribution (RMS error: 3.791%).

In addition to these probabilities, an average driving speed of 56kmh (35mph) and an average driving energy efficiency of 0.1305 kWh/kmh (0.21 kWh/mph) are taken from [27]. Using the predicted driving distance and average driving speed with the driving energy efficiency, it is possible to estimate an EV's energy demand upon arrival. Starting to charge from this arrival time until the energy demand has been met allowed to generate an estimated charging profile of a single EV. To do so, a maximum charging power of 5kW and an immediate disconnection of the EV upon charge completion was assumed.

Generating several of those charging profiles and aggregating them produces an estimated charging demand for an entire fleet of EVs. To provide an example, charge demand profiles for 50 EVs were generated, aggregated and plotted in Figure 3. This plot shows the expected magnitude and variability in energy demand that is required to charge several EVs at consumers' homes based upon the vehicles' daily useage. This data, was used to feed additional demand into the network models, which are outlined in the next section.

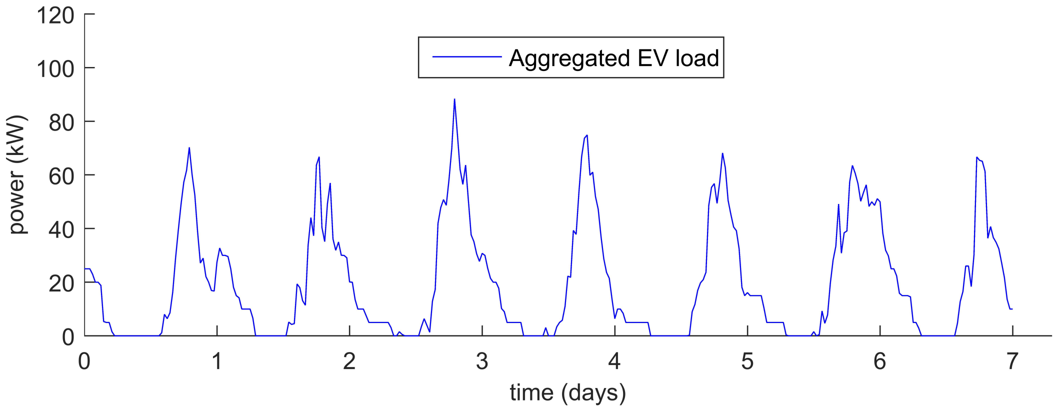

Figure 3. Excerpt from the aggregated 50 EVs, rated at 5kW, charging powers that were each generated from the empirical models.

2.3. Battery Modelling

For this work, a well established model that has been used in previous publications by this research group was used [25,28]. Typically, an ideal battery changes its State of Charge (SOC) depending on the power that flows into it, P_{bat}. When analysing the battery system at a regular sampling period τ, then the energy transferred into the system can be described as $P_{bat}\tau$. Optimally, the change in SOC, δ_{SOC}, can be described as follows:

$$\delta_{SOC}(t) = P_{bat}(t)\tau = \mathrm{SOC}(t) - \mathrm{SOC}(t-\tau) \tag{4}$$

Adding standby and conversion losses, respectively η_s and $\hat{\eta}_c$, the evolution in SOC can be summarised as follows:

$$\mathrm{SOC}(t) = (1-\eta_s)\mathrm{SOC}(t-\tau) + \hat{\eta}_c\delta_{SOC}(t) \tag{5}$$

Here, the conversion losses in the power electronics are reflected as an asymmetric efficiency, which depends on the direction of the flow of energy. This is done by charging the battery at a lower rate when consuming energy, and discharging it quicker when exporting energy. Mathematically, this can be represented as:

$$\hat{\eta}_c = \begin{cases} \eta_s & \text{if } \delta_{SOC}(t) \geq 0 \\ \frac{1}{\eta_s} & \text{if } \delta_{SOC}(t) < 0 \end{cases} \tag{6}$$

In addition, both the SOC and P_{bat} are restricted due to the devices energy storage capabilities and maximum charge and discharge rate. These limitations are captured in Equation 7 and Equation 8, respectively.

$$\mathrm{SOC}_{min} < \mathrm{SOC}(t) < \mathrm{SOC}_{max} \tag{7}$$

$$|P_{bat}(t)| \leq \mathrm{P}_{max} \tag{8}$$

2.4. Network Models

To simulate the low-voltage energy distribution grid, the Open Distribution System Simulator (OpenDSS) developed by the Electronic Power Research Institute (EPRI) was used. It requires element based network models, including line, load and transformer information, and generates realistic power flow results.

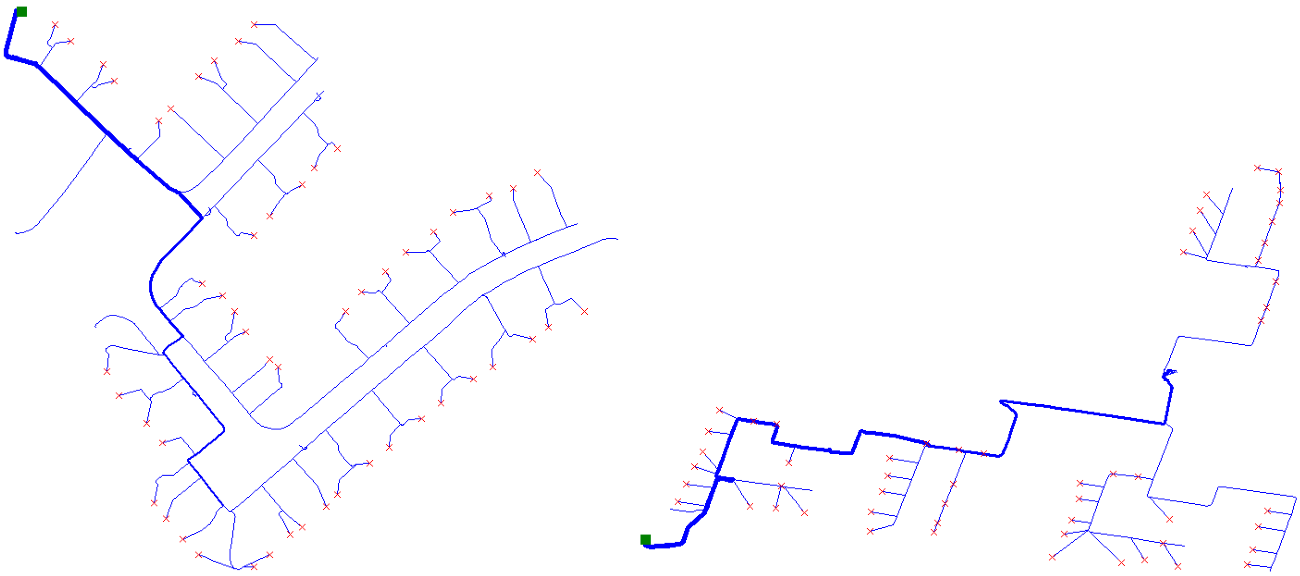

(a) IEEE PES EU Low Voltage Test Feeder with implicit neutral line simulation, 55 single-phase consumers and one substation.

(b) SSE-PD CIM based UK feeder with explicit neutral line simulation, 56 single-phase consumers and one substation.

Figure 4. Sample OpenDSS power flow plots of the used power networks. Consumers are indicated as red crosses and 11/0.416kV substations are marked with a green square.

The IEEE-PES's European Low Voltage Test Feeder was used for this work [29], and a set of detailed UK feeder models, provided by Scottish and Southern Energy Power Distribution (SSE-PD) were used, too. The SSE-PD circuit models were provided as Common Information Models (CIM) during the collaboration on the New Thames Valley Vision Project Project (NTVV) [30]. An example of the IEEE-PES EU LV Test feeder and a UK feeder provided by SSE-PD are shown in Figure 4a and Figure 4b, respectively.The model derived EV data and IEEE PES consumer demand profiles were used in all simulations. The resultant demand profiles represent the total daily electricity demand of households with EVs. These profiles were sampled at $\tau = 1$minute. The openDSS simulation environment is control using MATLAB. This was achieved through OpenDSS's Common Object Model (COM) interface and is accessible using Microsoft's ActiveX server bridge.

3. Storage Control

In this section, the control of the energy storage system is explained. Firstly, the Additive Increase Multiplicative Decrease (AIMD) algorithm is presented, then an improved voltage threshold is explained.

3.1. Additive Increase Multiplicative Decrease

The proposed distributed battery storage control is shown in Algorithm 1. The parameter α denotes the size of the power's Additive Increase step and β denotes the size of the Multiplicative Decrease step. The constants V_{max} and V_{thr} are used to regulate the total demand. More specifically, when the total demand is too high, the local voltages will drop below V_{thr} and the batteries will start to reduce their charging power or start discharging, in order to reduce total demand on the feeder. V_{max} is set to the nominal voltage of the substation transformer, $240V$, and V_{thr} is set to some fraction of V_{max}. The variable $V(t)$ is the local voltage and P_{max} denotes the maximum charging/discharging power of the battery.

Algorithm 1 Compute Battery Power

$R(t) = (V(t) - V_{thr})/(V_{max} - V_{thr})$ ▷ Defines the rate for the current voltage reading
if $V(t) \geq V_{thr}$ **then** ▷ Given the voltage levels are nominal...
  if $SOC < 0.9$ **then** ▷ ...and the battery is not fully charged...
    $P(t) = P(t - \tau) + \alpha P_{max} R(t)$ ▷ ...increase the charging power
  else ▷ If the battery has fully charged...
    $P(t) = 0$ ▷ ...shut off
  end if
  if $P(t) < 0$ **then** ▷ If the battery has been discharging...
    $P(t) = \beta P(t - \tau)$ ▷ ...quickly reduce the injected power
  end if
else ▷ If voltage levels are not nominal...
  if $SOC > 0.1$ **then** ▷ ...and battery is charged sufficiently...
    $P(t) = P(t - \tau) + \alpha P_{max} R(t)$ ▷ ...increase injected power
  else ▷ If the battery is not sufficiently charged...
    $P(t) = 0$ ▷ ...shut off
  end if
  if $P(t) > 0$ **then** ▷ If the battery has been charging...
    $P(t) = \beta P(t - \tau)$ ▷ ...quickly reduce the charging power
  end if
end if
$P(t) = \textbf{signum}(P(t)) \times \textbf{min}\{|P(t)|, P_{max}\}$ ▷ Limit the power to battery specifications, i.e. $\pm$2kW

The algorithm is characterised by two states of operation. During periods of low demand, the local voltage is higher than the threshold voltage and so the battery is set to charge. If the $V(t) < V_{thr}$ while charging, the rate, $R(t)$, becomes negative and the charging power of the battery is reduced. When demand is high and $V(t) < V_{thr}$ for a sustained period, then the battery begins to discharge. In contrast, if the $V(t) > V_{trr}$ while discharging, the rate, $R(t)$, becomes positive and the discharging power of the battery is reduced. The charging and discharging power of the batteries is incremented in proportion to the available headroom on the network, inferred from local voltage measurement $V(t)$. Yet with $V(t) \to V_{thr}$, the power increment for each battery is reduced to avoid sudden overload of the substation transformer.

3.2. Reference Voltage Profile

When using a fixed voltage threshold, the difference in location and load of each customer results in the over utilisation of batteries located at the feeder end. Similar to Papaioannou *et.al.* [31], a reference voltage profile is proposed, which is produced by performing a power flow analysis of the network, under maximum demand. An example of a fixed threshold and reference voltage profile is shown in Figure 5.

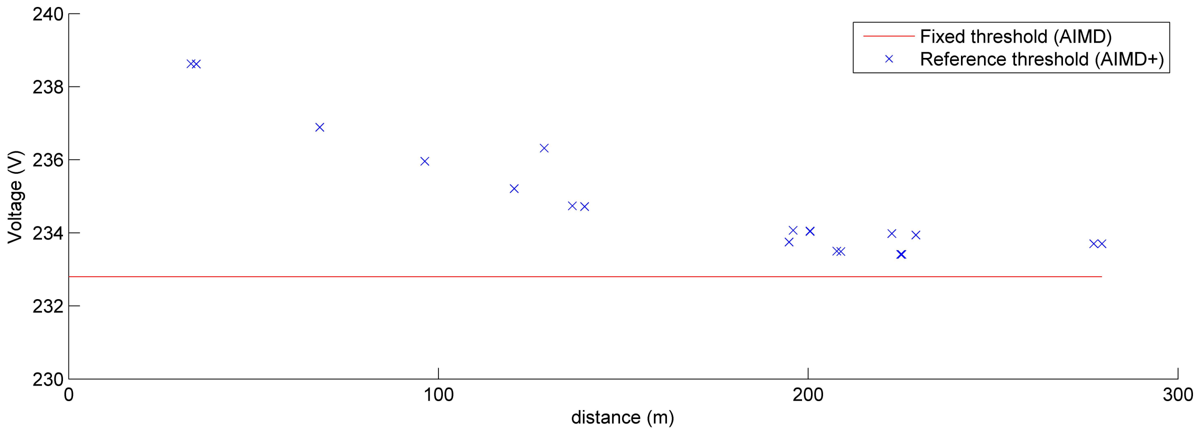

Figure 5. A plot showing the difference between the fixed voltage threshold (AIMD) and the reference voltage profile (AIMD+)

In the enhanced AIMD algorithm (AIMD+), consumers located at the head of the feeder are allocated a higher voltage threshold, while those towards the end of the feeder have similar voltage thresholds to that of the fixed threshold. This replicates the expected voltage drop along the length of the feeder and so results in a fairer utilisation of battery storage units, that are located at those distances. The voltage threshold is set so as to limit maximum voltage drop to 3% at the end of the feeder.

4. Scenarios and Comparison Metrics

In this section, several scenarios are explained that were used to test the performance of the battery control algorithm. Following that is a definition of three comparison metrics. These metrics quantify the improvements caused by the different algorithms in comparison to the worst case scenario.

4.1. Test Cases and Scenarios

In simulations the Electric Vehicles plug-in on arrival and charge at rate of 5kW until fully charged. The battery energy storage devices have a capacity of 7kWh with a maximum power rating of 2kW. Four test cases were defined with different levels EV and storage uptakes as follows:

A A baseline scenario, where only historic household demand is used.

B A worst case scenario, in which Electric Vehicle uptake is 100% and no battery energy storage is used.

C An AIMD scenario, in which Electric Vehicle uptake is 100% and each household has a battery energy storage device. Here, each battery was controlled using the AIMD algorithm using a fixed voltage threshold.

D An AIMD+ scenario, in which Electric Vehicle uptake is 100% and each household has a battery energy storage device. Here, each battery was controlled using the AIMD+ algorithm using the reference voltage profile.

A storage uptake of 100% was adopted to represent the worst case scenario. In addition to the four defined scenarios, a full set of simulations was performed with EV and storage uptake combinations of 0% to 100% in steps of 10%.

4.2. Performance Metric Definition

To obtain comparable performance metrics, three parameters are defined. These parameters capture the improvements in voltage violation mitigation, line overload reduction and fairness of battery usage. The excerpt performance metrics were calculated based on simulations from the IEEE EU test case for reproducibility .

4.2.1. Parameter for voltage improvement

The first parameter, ζ^*, calculates the magnitude of the voltage level improvement by comparing two voltage frequency distributions. More specifically, it finds the difference between these probability distributions and computes a weighted sum. Here, the weighting, $\delta^*(v)$, emphasises the voltage level improvements that deviate more from the nominal substation voltage V_{ss}. If the resulting weighted sum is negative, then the obtained voltage frequency distribution has improved in comparison to the associated worst case scenario. In contrast, a positive number would indicate a worse outcome. The performance metric is defined in Equation 9.

$$\zeta^*_{\mathbf{C}} := \sum_{v=V_{min}}^{V_{max}} \delta^*(v) \left[P_{\mathbf{B}}(v) - P_{\mathbf{C}}(v) \right] \tag{9}$$

Here, V_{min} is the lowest recorded voltage and V_{max} is the highest recorded voltage. $P_{\mathbf{B}}(v)$ is the voltage probability distribution of the worst case scenario (case **B**), and $P_{\mathbf{C}}(v)$ is the voltage probability distributions of case **C** (i.e. the case with maximum EV and AIMD storage uptake). Cases **B** and **D** would therefore be compared by parameter $\zeta^{*}_{\mathbf{D}}$.

The aforementioned factor, $\delta^{*}(v)$, scales down the summation in Equation 9 for voltages within the nominal operating band, as no voltage violations take place. Voltage violations are scaled up to increase their impact on the summation. This scaling was produced using a linear function, symmetric about V_{ss}, that is defined as:

$$\delta^{*}(v) := \begin{cases} \frac{V_{ss}-v}{V_{ss}-V_{low}} & \text{if } v \leq V_{ss} \\ \frac{v-V_{ss}}{V_{high}-V_{ss}} & \text{otherwise} \end{cases} \tag{10}$$

where, V_{low} and V_{high} are defined as the lower and upper limits of the nominal operation voltage band, respectively. In general, the proposed voltage comparison parameter, ζ^{*}, shows an improvement in voltage distribution when it is negative, whereas a positive value implies a voltage distribution with more voltage violations.

4.2.2. Parameter for line overload reduction

Similar to measuring the voltage level improvements, the line utilisation probability distributions between the storage and worst case scenarios were compared. This follows a similar equation described in Equation 9, but using a different scaling factor:

$$\zeta^{**}_{\mathbf{C}} := \sum_{c=0}^{C_{max}} \delta^{**}(c)\left[P_{\mathbf{C}}(c) - P_{\mathbf{B}}(c)\right] \tag{11}$$

Here, C_{max} is the highest line utilisation. $P_{\mathbf{B}}(c)$ and $P_{\mathbf{C}}(c)$ are the line utilisation probability distributions for case **B** and **C**, respectively, and $\delta^{**}(c)$ is the associated scaling factor. Since the relationship between line current and ohmic losses is quadratic, this scaling factor is defined as an exponential function that amplifies the impact of line currents beyond the line's nominal rating.

$$\delta^{**}(c) = \begin{cases} \left(\frac{c}{1-C_{min}}\right)^{2} & \text{if } c \geq C_{min} \\ 0 & \text{otherwise} \end{cases} \tag{12}$$

The modifier C_{min} defines from where the scaling should start and has been set to 0.5 for this work as only line utilisation above 0.5 p.u. was considered. Therefore, a reduction in line overloads would gives a negative ζ^{**}, whereas a positive value implies a higher line utilisation.

4.2.3. Parameter for improvement of battery cycling

The final metric, ζ^{***}, gives an indication of the inequality of battery cycling across all battery units. It does this by computing the the ratio between the peak and mean battery cycling. This Peak-to-Average Ratio (PAR) is defined in the following equation.

$$\zeta^{***}_{\mathbf{C}} := \frac{\max|C_{\mathbf{C}}|}{B^{-1}\sum_{b=1}^{B}\left|c^{b}_{\mathbf{C}}\right|} \tag{13}$$

Here, B is the number of batteries and $c^b_{\mathbf{C}}$ is the total cycling of battery b during scenario **C**. $C_{\mathbf{C}}$ is a vector of $\mathbb{R}^B_{\geq 0}$, that contains all batteries' cycling values, i.e. $c^b_{\mathbf{C}} \in C_{\mathbf{C}}$. Equally, the battery cycling for scenario **D** would be captured by $\zeta^{***}_{\mathbf{D}}$. In the unlikely event of an equal cycling of all batteries, ζ^{***} will have a value of one. Yet as batteries are operated differently, the value of ζ^{***} is likely to be greater than one. Therefore, a resulting PAR closer to one implies a more equal and therefore fairer utilisation of the deployed batteries.

5. Results and Discussion

In this section, the results are outlined that were generated from all simulations. In each of the three subsections, the performances of the AIMD and AIMD+ algorithm are compared against another. To do so, the performance metrics outlined in Section 4.2 are used. In each subsection, results from the four test cases defined as **A**, **B**, **C** and **D** in Section 4.1 are explained first, then the results from the full analysis over the large range of EV and battery storage uptake is presented. In the end, these results are put into context and discussed.

5.1. Voltage Violation Analysis

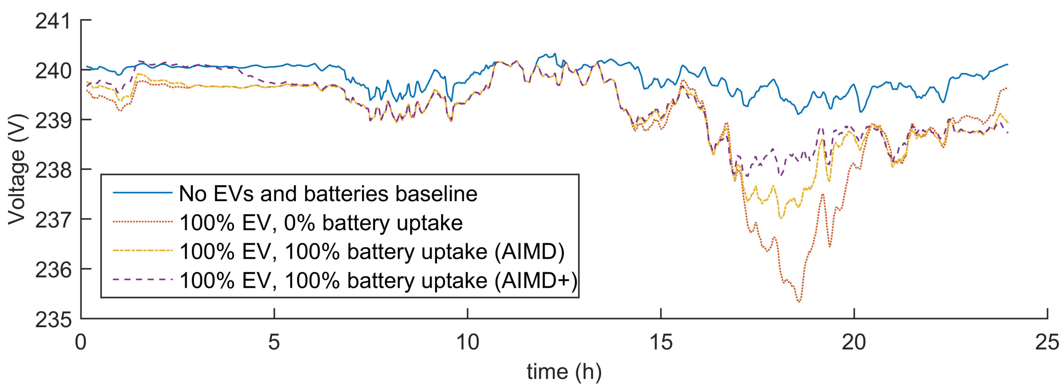

Figure 6. Recorded voltage profile at the first consumer's bus over the period of one with a certain uptake in EV and battery storage devices using a moving average over a window of 5 minutes. Here, case **A** is blue, case **B** is red, case **C** is yellow, and case **D** is violet.

The results were compared based on their performance at improving the voltage profile of the feeder, by increasing the minimum voltage recorded at each bus. Each load's bus voltage was recorded, from which a sample voltage profile, Figure 6, was extracted, where the bus voltage fluctuation over time becomes apparent. Here, the introduction of EVs has significantly lowered the line-to-neutral voltage. Adding energy storage devices has raised the voltage levels during times of peak demand, as can be seen between 17:00 - 21:00,where the AIMD+ algorithm has elevated voltages further than AIMD scenario. To obtain a better understanding of the level of improvement, the voltage frequency distribution for the entire feeder was generated and plotted in a histogram in Figure 7.

In this histogram, the voltage probability distribution for all four cases were normalised and plotted against another. Here, the previously seen drop in voltages by introducing EVs is recorded as a shift in the voltage distribution. This voltage drop is impacted by the introduction of the storage solutions,

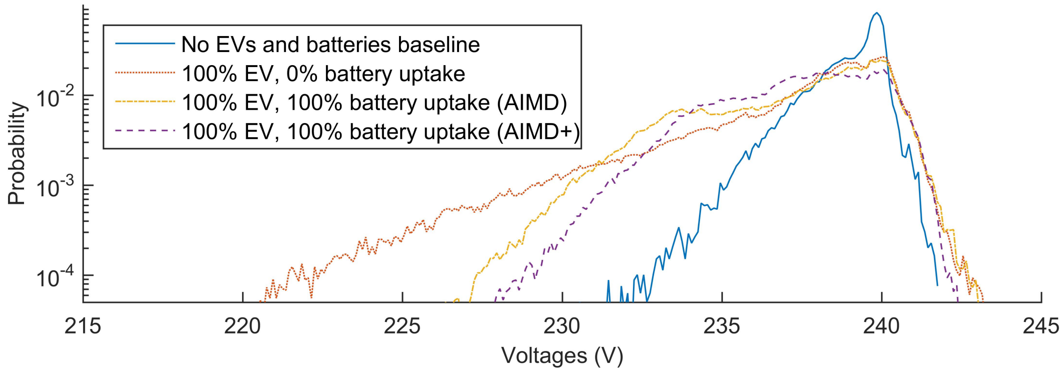

Figure 7. Voltage probability distribution of all loads' buses for certain uptakes of EV and battery storage devices. Here, case **A** is blue, case **B** is red, case **C** is yellow, and case **D** is violet with $\zeta^*_{\mathbf{C}} = -0.0128$ and $\zeta^*_{\mathbf{D}} = -0.0362$.

since the probability distribution is shifted towards higher voltage bands. For the IEEE PES test case, the AIMD+ controlled batteries outperform the AIMD devices as the resulting $\zeta^*_{\mathbf{C}}$ is greater than $\zeta^*_{\mathbf{D}}$.

To gain a full understanding of the performance of the AIMD and AIMD+ algorithms, a full sweep of EV and storage uptake combinations was simulated on all available power distribution networks. The resulting parameters were averaged and plotted in Figure 8.

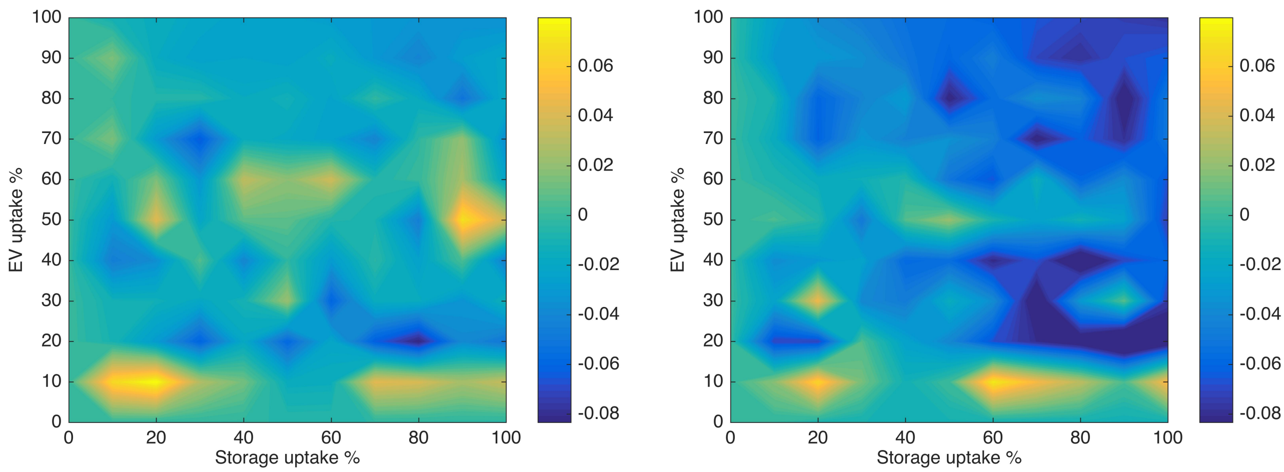

(a) $\zeta^*_{\mathbf{C}}$ indices (AIMD) **(b)** $\zeta^*_{\mathbf{D}}$ indices (AIMD+)

Figure 8. Comparison of voltage improvement indices (i.e. ζ^*) for AIMD (Fig. 8a) and AIMD+ (Fig. 8b).

These figures show that the AIMD+ control algorithm reduces voltage variation as the uptake in storage and EVs increases. The AIMD algorithm does not perform as effectively since more $\zeta^*_{\mathbf{C}}$ values are positive and larger than their corresponding $\zeta^*_{\mathbf{D}}$ value. This becomes more apparent when removing the EV uptake axis and averaging all $\zeta^*_{\mathbf{C}}$ and $\zeta^*_{\mathbf{D}}$ values for a their common storage uptake. The resulting averaged metrics are plotted in Figure 9.

In this last figure the it can be seen how an increase in battery uptake impacts the improvement of voltage levels. In fact, both compared algorithms improved the bus voltage distributions, yet the AIMD+ algorithm noticeably outperformed the AIMD algorithm. This is the case as for every uptake $\zeta^*_{\mathbf{C}} > \zeta^*_{\mathbf{D}}$.

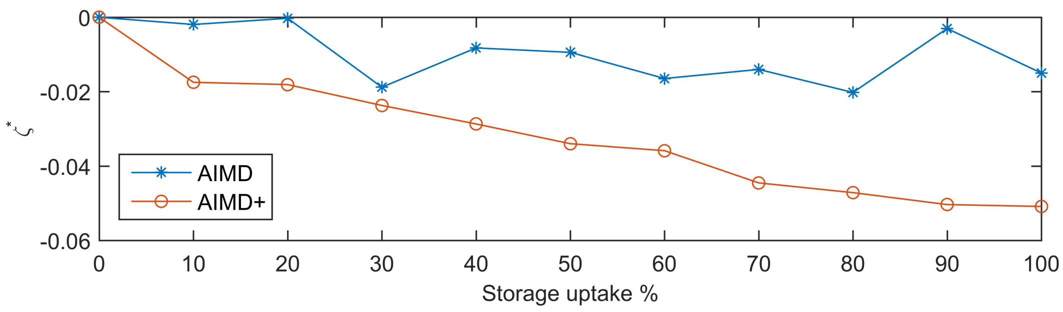

Figure 9. Average $\zeta^*_{\mathbf{C}}$ (AIMD) and $\zeta^*_{\mathbf{D}}$ (AIMD+) values recorded against the corresponding storage uptake.

5.2. Line Overload Analysis

Similar to the voltage improvement analysis, a frequency distribution of the line utilisation was generated. Figure 10 is shows a probability distribution of the per unit current in all lines, for each of the four scenarios. The corresponding $\zeta^{**}_{\mathbf{C}}$ and $\zeta^{**}_{\mathbf{D}}$ values for the AIMD and AIMD+ storage deployment have also been included in the figure's caption.

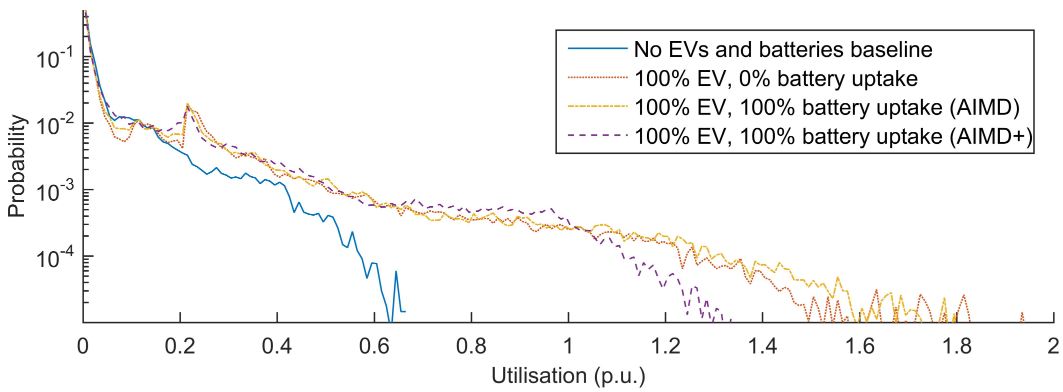

Figure 10. Line utilisation probability distribution of all lines in the simulated feeder for certain uptakes of EV and battery storage devices. Here, case **A** is blue, case **B** is red, case **C** is yellow, and case **D** is violet with $\zeta^{**}_{\mathbf{C}} = 0.174$ and $\zeta^{**}_{\mathbf{D}} = -0.364$.

Here, the AIMD+ controlled storage devices show a reduction in line overloads. This improvement is noticeable through the compressed width of the probability distribution and negative $\zeta^{**}_{\mathbf{D}}$ value. In contrast, the AIMD controlled storage devices do not fully utilise the line capacity as effectively, which leads to a positive value of $\zeta^{**}_{\mathbf{C}}$. To evaluate the line utilisation improvement across all simulations, the full range of EV and storage uptake was evaluated. The resulting plots are shown in Figure 11.

In these figures, it can be seen how the performance metrics change as EV and storage uptake increases. For the AIMD controlled batteries the resulting $\zeta^{**}_{\mathbf{C}}$ values are distributed around zero, whereas the AIMD+ algorithm achieved mostly negative values of $\zeta^{**}_{\mathbf{D}}$. These negative values confirm the higher utilisation of line capacity. This becomes more noticeable for scenarios where very low EV uptake is combined with very large storage uptake. Here, AIMD controlled storage devices commence their initial charge simultaneously, which causes a number of line overloads. The AIMD+ algorithm increases the charging gradually, preventing these line overloads from occurring.

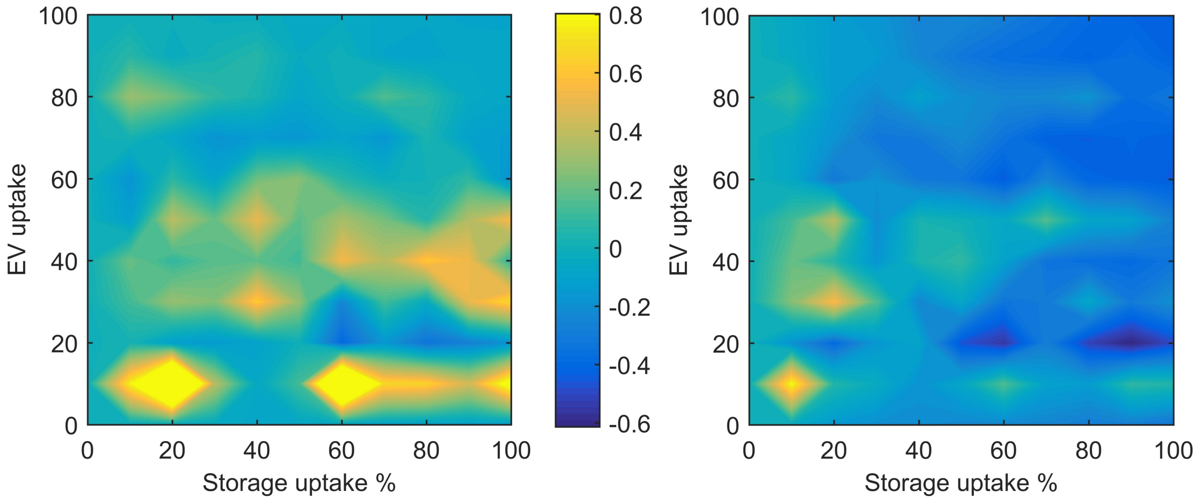

(a) $\zeta_{\mathbf{C}}^{**}$ indices (AIMD) **(b)** $\zeta_{\mathbf{D}}^{**}$ indices (AIMD+)

Figure 11. Comparison of line utilisation improvement indices for AIMD (Fig. 11a) and AIMD+ (Fig. 11b).

Averaging the $\zeta_{\mathbf{C}}^{**}$ and $\zeta_{\mathbf{D}}^{**}$ values over all EV uptakes gives an clearer indication of performance, as this is now the only variable in the performance analysis. The result is plotted in Figure 12. Here, the hypothesis that AIMD controlled energy storage devices do not improve line utilisation is confirmed. In contrast, the AIMD+ controlled devices succeed at reducing line overloads. This is also demonstrated by the values of $\zeta_{\mathbf{C}}^{**}$, which remains positive yet close to zero, whereas $\zeta_{\mathbf{D}}^{**}$ decreases with increasing uptake of battery storage devices.

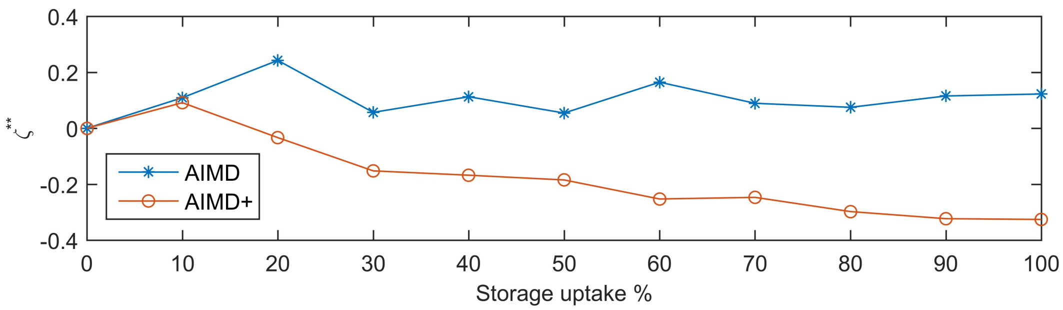

Figure 12. Average $\zeta_{\mathbf{C}}^{**}$ (AIMD) and $\zeta_{\mathbf{D}}^{**}$ (AIMD+) values recorded against the corresponding storage uptake.

Whereas the deployment of energy storage has often been seen as a possible solution to defer network reinforcements, the presented results show that this is not the case. In fact, the importance of choosing an appropriate control algorithm outweighs the availability of the energy storage itself. This becomes particularly apparent when energy storage devices need to recharge their injected energy for times of peak demand. For the AIMD case, this recharging is not controlled sufficiently, which leads to higher line currents. The proposed AIMD+ algorithm was not as susceptible to this kind of behaviour as it is designed to take battery location into account. This immunity and the well controlled power injection causes very little to no additional strain on the network's equipment, yet allows the deployed storage devices to provide voltage support.

5.3. Battery Utilisation Analysis

In this part of the analysis, the batteries' fairness of usage was evaluated. The battery power profiles were recorded and an excerpt has been plotted in Figure 13. These power profiles are arranged by distance from the substation.

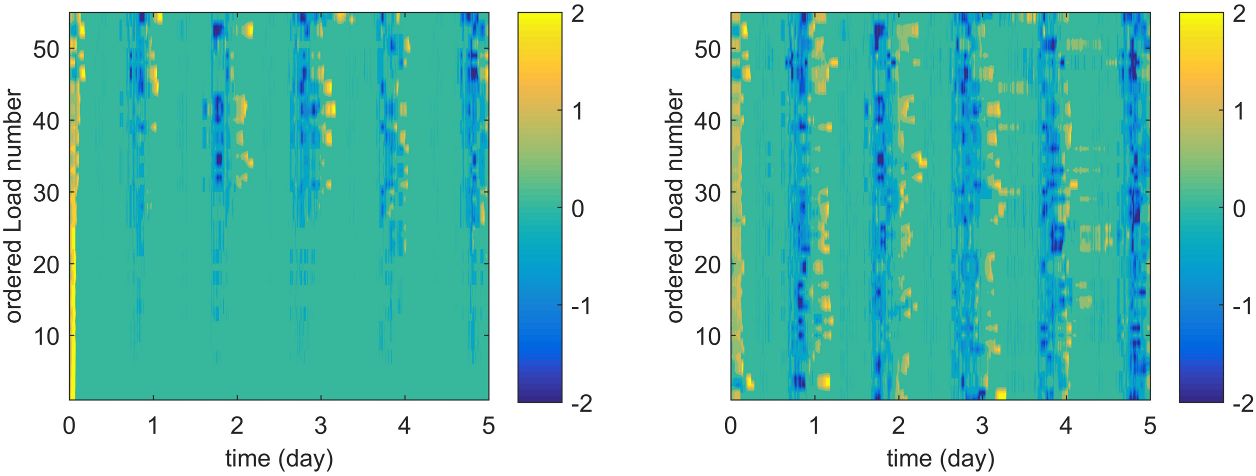

(a) Case **C** - 60% EV and 100% AIMD (kW) **(b)** Case **D** - 60% EV and 100% AIMD+ (kW)

Figure 13. Battery power profiles of each load's battery storage device over four days for AIMD (Fig. 13a) and AIMD+ (Fig. 13b).

In this figure, it can be seen that only half of the deployed storage devices were active in case **C** (AIMD control), whereas nearly all devices are utilised in case **D** (AIMD+ control). From the recorded battery SOC profiles, the net cycling of each battery was computed and divided by the duration of the simulation, giving an average daily cycling value. This is plotted for each load in Figure 14a. The corresponding statistical analysis is presented in Figure 14b.

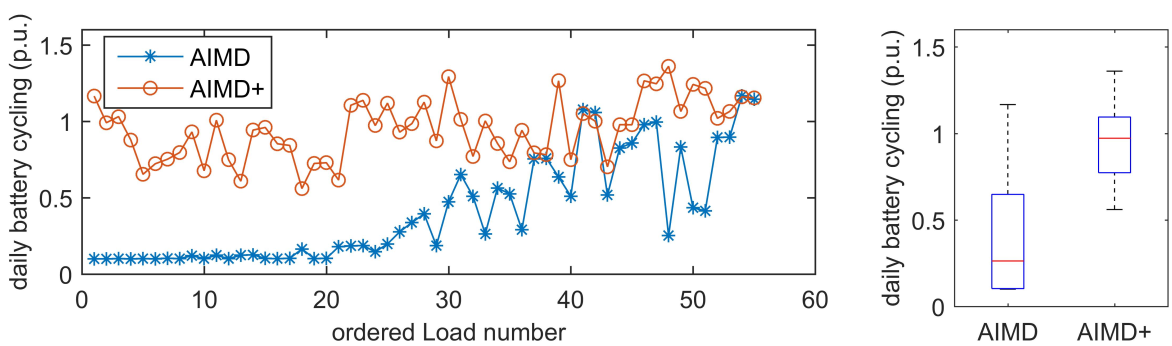

(a) Battery cycling for each load **(b)** Statistics

Figure 14. Each load's battery cycling compared for 60% EV and 100% AIMD and AIMD+ uptake (Fig. 14a) and in a statistical context (Fig. 14b). Here, $\zeta^{***}_{\mathbf{C}} = 3.51$ and $\zeta^{***}_{\mathbf{D}} = 1.61$

These two plots show the under-usage of AIMD controlled batteries as well as the imbalance in battery usage under AIMD and AIMD+ control. In fact, under AIMD control, 20 out of 55 batteries experience a cycling of less than 10% per day whereas the remaining devices are utilised more fully. This discrepancy causes the $\zeta_{\mathbf{C}}^{***}$ value to be noticeably larger than $\zeta_{\mathbf{D}}^{***}$. A more detailed comparison was performed by plotting the Peak-to-Average Ratios from the full range of EV and storage uptake scenarios and plotted in Figure 15.

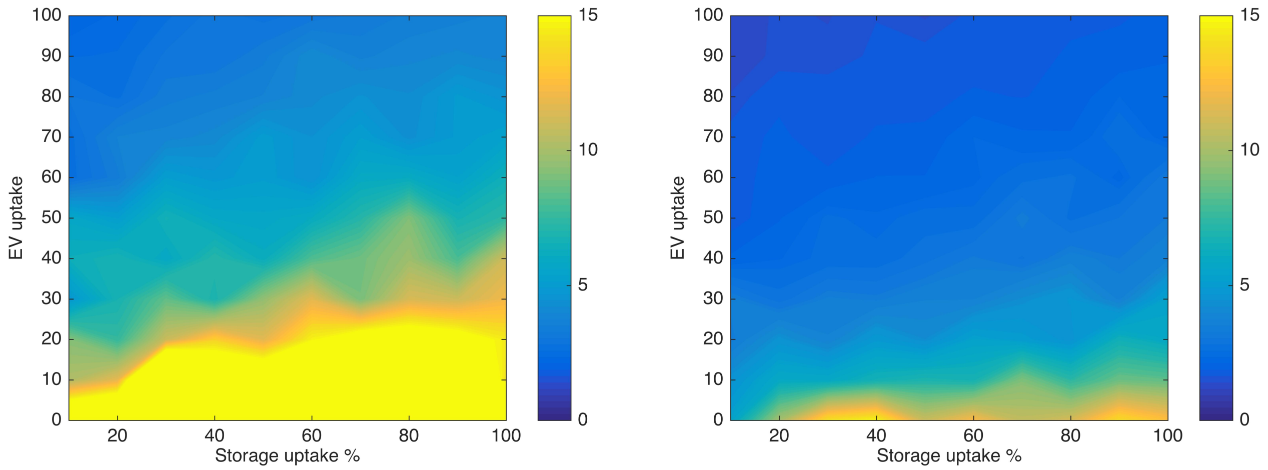

(a) Case **C** - 60% EV and 100% AIMD

(b) Case **D** - 60% EV and 100% AIMD+

Figure 15. Battery power profiles of each load's battery storage device over four days for AIMD (Fig. 15a) and AIMD+ (Fig. 15b).

This figure shows that for any EV uptake scenario, AIMD controlled energy storage units were cycled less equally than the AIMD+ controlled devices. Results show that with a low uptake of EVs, both the AIMD and AIMD+ algorithm performed worse, improving as electric vehicle uptake is increased. Removing Electric Vehicle uptake from the analysis, the performance difference between AIMD and AIMD+ becomes more visible. The resulting averaged $\zeta_{\mathbf{C}}^{***}$ and $\zeta_{\mathbf{D}}^{***}$ values for their corresponding storage uptake percentages are presented in Figure 16.

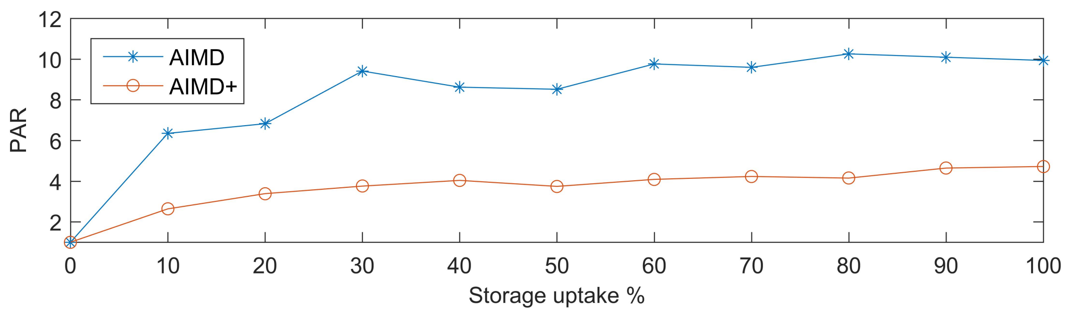

Figure 16. The performance index $\zeta_{\mathbf{C}}^{***}$ for AIMD storage and $\zeta_{\mathbf{D}}^{***}$ for AIMD+ storage control against storage uptake.

Although the AIMD controlled batteries were, on average, cycled less than the batteries controlled by the proposed AIMD+ algorithm, just looking at the average produces a distorted understanding of the performance. In fact, as more than half of the assigned AIMD energy storage devices never partook in the network control, a lower average cycling is expected. The variation in cycling across all batteries, or the cycling Peak-to-Average Ratio, reveals the difference between usage and effective usage. The lower ratio indicating a better usage of the deployed batteries.

6. Conclusions

In this paper, a distributed battery energy storage algorithm for mitigation of uncontrolled loads, such as the charging of Electric Vehicles, is proposed. The proposed AIMD+ algorithm uses local bus voltage measurements and a reference voltage profile derived from power flow analysis of the distribution network. The addition of the reference profile takes into consideration the distance of the battery units to their feeding substation and is used to determine the rate of power increase when charging and discharging the battery. Simulations were performed on the IEEE European test case and a set of real UK suburban networks. Comparisons were made of the standard AIMD algorithm with fixed voltage threshold against the proposed AIMD+ algorithm using a reference voltage threshold. A set of European demand profiles and realistic electric vehicle travel model were used.

For the conducted simulations, the AIMD controlled energy storage performance was improved by using the computed reference voltage profile. The improved AIMD algorithm resulted in a reduction of voltage variation and an increased utilisation of available line capacity, which also reduced the frequency of line overloads. Additionally, the same algorithm equalised cycling and utilisation of battery energy storage, making most use of the deployed battery assets. To take this work further, future work will also consider distributed generation, such as photovoltaic panels (PV), beside electric vehicle uptake, as well as decentralised methods for determining voltage reference values so no prior network knowledge is required.

Acknowledgments

The authors would like to thank SSE-PD for providing the network information for the utilised UK feeder models.

Author Contributions

The two lead authors contributed equally to this piece of work and were supervised by Dr William Holderbaum and Dr Ben A. Potter.

Conflicts of Interest

The authors declare no conflict of interest.

References

1. Shah, V.; Booream-Phelps, J. F.I.T.T. for Investors: Crossing the Chasm. Technical report, 2015.
2. Department for Business Enterprise and Regulatory (DBER).; Department for Transport (DfT). Investigation into the Scope for the Transport Sector to Switch to Electric Vehicles and Plug- in Hybrid Vehicles. Technical report, 2008.

3. Ecolane.; University of Aberdeen. Pathways to high penetration of electric vehicles. Technical report, 2013.
4. Clement-Nyns, K.; Haesen, E.; Driesen, J. The impact of Charging plug-in hybrid electric vehicles on a residential distribution grid. *IEEE Trans. Power Syst.* **2010**, *25*, 371–380.
5. Pieltain Fernández, L.; Gómez San Román, T.; Cossent, R.; Mateo Domingo, C.; Frías, P. Assessment of the impact of plug-in electric vehicles on distribution networks. *IEEE Trans. Power Syst.* **2011**, *26*, 206–213.
6. Hadley, S.W.; Tsvetkova, A.a. Potential Impacts of Plug-in Hybrid Electric Vehicles on Regional Power Generation. *Electr. J.* **2009**, *22*, 56–68.
7. Putrus, G.; Suwanapingkarl, P.; Johnston, D.; Bentley, E.; Narayana, M. Impact of electric vehicles on power distribution networks. 2009 IEEE Veh. Power Propuls. Conf., 2009, pp. 827–831.
8. Pillai, J.R.; Bak-Jensen, B. Vehicle-to-grid systems for frequency regulation in an islanded Danish distribution network. *2010 IEEE Veh. Power Propuls. Conf. VPPC 2010* **2010**.
9. Zhou, K.; Cai, L. Randomized PHEV Charging Under Distribution Grid Constraints. *IEEE Trans. Smart Grid* **2014**, *5*, 879–887.
10. Mohsenian-Rad, A.H.; Wong, V.W.S.; Jatskevich, J.; Schober, R.; Leon-Garcia, A. Autonomous demand-side management based on game-theoretic energy consumption scheduling for the future smart grid. *IEEE Trans. Smart Grid* **2010**, *1*, 320–331.
11. Deilami, S.; Masoum, A.S. Real-time coordination of plug-in electric vehicle charging in smart grids to minimize power losses and improve voltage profile. *IEEE Trans. Smart Grid* **2011**, *2*, 456–467.
12. Masoum, A.S.; Deilami, S.; Member, S.; Masoum, M.A.S.; Member, S. Fuzzy Approach for Online Coordination of Plug-In Electric Vehicle Charging in Smart Grid. *IEEE Trans. Sustain. Energy* **2015**, *6*, 1112–1121.
13. Karfopoulos, E.L.; Hatziargyriou, N.D. A Multi-Agent System for Controlled Charging of a Large Population of Electric Vehicles. *IEEE Trans. Power Syst.* **2013**, *28*, 1196–1204.
14. Wu, C.; Mohsenian-Rad, H.; Huang, J. Vehicle-to-aggregator interaction game. *IEEE Trans. Smart Grid* **2012**, *3*, 434–442.
15. Samadi, P.; Mohsenian-Rad, H.; Schober, R.; Wong, V.W.S. Advanced Demand Side Management for the Future Smart Grid Using Mechanism Design. *IEEE Trans. Smart Grid* **2012**, *3*, 1170–1180.
16. Xu, N.Z.; Chung, C.Y. Challenges in Future Competition of Electric Vehicle Charging Management and Solutions. *IEEE Trans. Smart Grid* **2015**, *6*, 1323–1331.
17. Chiu, D.M.; Jain, R. Analysis of the increase and decrease algorithms for congestion avoidance in computer networks, 1989.
18. Stüdli, S.; Crisostomi, E.; Middleton, R.; Shorten, R. A flexible distributed framework for realising electric and plug-in hybrid vehicle charging policies. *International Journal of Control* **2012**, *85*, 1130–1145.
19. Stüdli, S.; Crisostomi, E.; Middleton, R.; Shorten, R. Optimal real-time distributed V2G and G2V management of electric vehicles. *Int. J. Control* **2014**, *87*, 1153–1162.

20. Stüdli, S.; Crisostomi, E.; Middleton, R.; Braslavsky, J.; Shorten, R. Distributed Load Management Using Additive Increase Multiplicative Decrease Based Techniques. In *Plug Electr. Veh. Smart Grids*; Springer Singapore, 2015; pp. 173–202.
21. Mareels, I.; Alpcan, T.; Brazil, M.; de Hoog, J.; Thomas, D.a. A distributed electric vehicle charging management algorithm using only local measurements. Innov. Smart Grid Technol. Conf. (ISGT), 2014 IEEE PES; , 2014; pp. 1–5.
22. Munkhammar, J.; Bishop, J.D.; Sarralde, J.J.; Tian, W.; Choudhary, R. Household electricity use, electric vehicle home-charging and distributed photovoltaic power production in the city of Westminster. *Energy Build.* **2015**, *86*, 439–448.
23. Dallinger, D.; Wietschel, M. Grid integration of intermittent renewable energy sources using price-responsive plug-in electric vehicles. *Renew. Sustain. Energy Rev.* **2012**, *16*, 3370–3382.
24. Infas.; Deutsches Zentrum für Luft- und Raumfahrt e.V. Mobilität in Deutschland 2008. Technical report, Bonn und Berlin, Deutschland, 2008.
25. Rowe, M.; Member, S.; Yunusov, T.; Member, S.; Haben, S.; Singleton, C.; Holderbaum, W.; Potter, B. A Peak Reduction Scheduling Algorithm for Storage Devices on the Low Voltage Network. *IEEE Trans. Smart Grid* **2014**, *5*, 2115–2124.
26. Laresgoiti, I.; Käbitz, S.; Ecker, M.; Sauer, D.U. Modeling mechanical degradation in lithium ion batteries during cycling: Solid electrolyte interphase fracture. *J. Power Sources* **2015**, *300*, 112–122.
27. UK Government Digital Service. Vehicle free-flow speeds (SPE01), 2013.
28. Rowe, M.; Yunusov, T.; Haben, S.; Holderbaum, W.; Potter, B. The real-time optimisation of DNO owned storage devices on the LV network for peak reduction. *Energies* **2014**, *7*, 3537–3560.
29. Society, I.P.; Energy. European Low Voltage Test Feeder, 2015.
30. Thames Valley Vision. http://www.thamesvalleyvision.co.uk. Accessed: 2016-01-27.
31. Papaioannou, I.T.; Purvins, A.; Demoulias, C.S. Reactive power consumption in photovoltaic inverters: a novel configuration for voltage regulation in low-voltage radial feeders with no need for central control. *Progress in Photovoltaics: Research and Applications* **2015**, *23*, 611–619.